

Flux assisted low-temperature synthesis of YAG : Yb³⁺,Er³⁺ and its optical property

Suk Hyun Kang^a, Jeong Ho Ryu^b, Cheol Woo Park^a, Jae Hwa Park^a, Hyun Mi Kim^a, Hyo Sang Kang^a,
Jae Sang Choi^a, Joo Hyun Jung^a, Bong Geun Choi^a and Kwang Bo Shim^{a,*}

^aDivision of advanced Materials Science and Engineering, Hanyang University, Seoul 133-791, Korea

^bDepartment of Materials Science and Engineering, Korea National University of Transportation, Chungbuk 380-702, Korea

Yb³⁺/Er³⁺ co-doped polycrystalline yttrium-aluminum garnet (YAG : Yb³⁺,Er³⁺) powders were synthesized by a flux (BaF₂) assisted solid-state reaction method at low-temperature. The optimum condition of flux concentration and calcination temperature was investigated by the XRD analysis. Crystal structure and upconversion luminescent property of the synthesized YAG : Yb³⁺,Er³⁺ powder was analyzed as a function of Yb³⁺ concentration when concentration of Er³⁺ was fixed at 25.0 mol%. Under 980 nm excitation, YAG : Yb³⁺,Er³⁺ powder exhibited weak red emissions near 660 and 670 nm, and strong green UC emissions at 530 and 550 nm corresponding to the intra 4f transitions of Er³⁺ (⁴F_{9/2}, ²H_{11/2}, ⁴S_{3/2}) → Er³⁺ (⁴I_{15/2}). The Yb³⁺ 15 mol% doped YAG : Yb³⁺,Er³⁺ powder sample exhibited strongly shiny green emission. A possible UC mechanism for YAG : Yb³⁺,Er³⁺ depending was discussed in detail.

Key words: BaF₂ flux, YAG : Yb³⁺,Er³⁺, upconversion.

Introduction

Yttrium-aluminum garnet (YAG or Y₃Al₅O₁₂) has important optical properties, which have been used as hosts for lasers and phosphor materials [1, 2]. The yttrium-aluminum matrix presents three crystalline phases; two stable Y₃Al₅O₁₂ or Y₄Al₂O₉, and metastable YAlO₃ [3, 4]. Recently, ceramic crystalline ceramic lasers appear extensively in the This is an literatures because they can lead to materials with excellent optical characteristics [5-7], especially Nd:YAG single crystal [8, 25-27].

Powders with pure YAG phase are usually synthesized by a conventional solid-state reaction method with Y₂O₃ and Al₂O₃ as the raw materials [9, 10]. This is an efficient and cost-effective method as compared with other complex synthetic routes. However, this method has a few inherent disadvantages in that it requires a high calcination temperature over 1600 °C and long processing time..

In light of these issues, this study mainly focuses on developing a novel solid-state reaction route at low temperature to synthesize crystalline YAG : Yb³⁺,Er³⁺ powders. To overcome the drawbacks of the conventional solid-state reaction method and to achieve phase purity, we prepared an initial mixture using raw oxide powders combined with BaF₂, which is known as proper flux in the synthesis of YAG powders [11, 12, 28] and the upconversion luminescent mechanism of the synthesized YAG : Yb³⁺,Er³⁺ will discussed.

Experimental

The nominal composition of the phosphor is Y_{3-x-y}(Er_x)(Yb_y)Al₅O₁₂. The raw materials are high purity grade Y₂O₃, Al₂O₃, Er₂O₃ and Yb₂O₃. BaF₂ as flux is added to the starting materials with weight percentage from without to 10.0 wt%. All of them are purchased from Kojundo Chemicals Co., Ltd., with reagent grade. The reactants were weighted stoichiometrically and thoroughly ground in a ball mill. Ethyl alcohol is added into the ball mill container and the weight ratio of ball, alcohol and powder is 3 : 3 : 1. The ball mill was operated at 200 rpm for 5 hrs and the mixture slurry is dried at 100 °C for 2 hrs. Then the mixed powders were put into alumina crucible. The alumina crucibles were fired at different temperatures from 700 to 1500 °C in air for 5 h and pulverized into fine powders in an agate mortar after cooling. The fine powders were washed by 80 °C water for removal of flux residue.

The phase analysis was conducted using X-ray diffraction (XRD, Rigaku D/MAX2C, Japan, Cu-α (λ = 1.5046 Å)). Room-temperature upconversion luminescent spectra originated from Er³⁺ were obtained using a photoluminescence spectrophotometer (PerkinElmer, LS55 with an IR laser diode (980 nm, 100 mW)) in a range of 400-700 nm.

Results and Discussion

Fig. 1(a) shows the XRD patterns of pure YAG powder prepared at 1500 °C for 5 hrs in air by a solid state reaction without and with a BaF₂ flux. XRD patterns of the samples illustrate that all of the samples

*Corresponding author:
Tel : +82-2-2290-0501
Fax : +82-2-2299-2884
E-mail: kbshim@hanyang.ac.kr

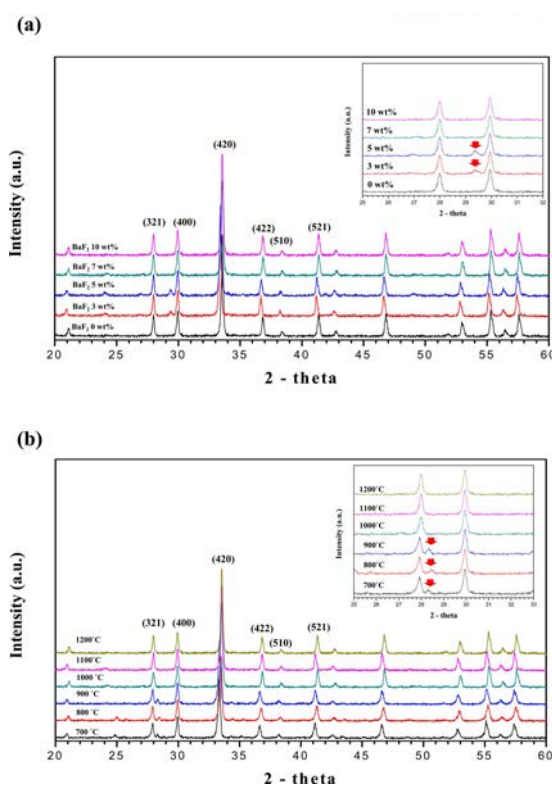


Fig. 1. XRD patterns of pure YAG samples prepared (a) at 1500 °C as a function of BaF₂ flux weight ratio and (b) from 700 to 1200 °C when the BaF₂ flux weight ratio is fixed at 7.0 wt%.

could be assigned a cubic crystalline structure (JCPDS No: 33-0040). The XRD patterns for the samples obtained without and with the BaF₂ flux were similar to each other. No distinct XRD peaks corresponding to BaF₂ were observed, which indicates that most of the BaF₂ flux was removed through washing process. For understanding the effect of BaF₂ on the crystallinity of the YAG phase, the relative intensity of the main diffraction peak (4 2 0) and existence of secondary peaks were examined. When the pure YAG phase was synthesized at 1500 °C without and with BaF₂ flux up to 5.0 wt%, unreacted secondary peaks around 29.5° were detected as shown in inset of Fig. 1(a). Moreover, relative intensity of diffraction peaks was improved as the weight ratio of the BaF₂ flux increase. The YAG sample synthesized with 7.0 wt% BaF₂ shows single crystalline XRD peaks without any secondary or unreacted phase. Therefore we could conclude that the optimum weight ratio for the BaF₂ flux is 7.0 wt%.

Fig. 1(b) shows the XRD patterns of pure YAG powder from 700 to 1200 °C for 5 hrs in air when BaF₂ weight ratio is fixed at 7.0 wt%. XRD patterns of the samples illustrate that all of the samples could be assigned a cubic crystalline structure. The XRD patterns for the samples obtained at various temperature were similar to each other. For understanding the effect of heat treatment temperature on the crystallinity of the YAG phase, the relative intensity of the main diffraction peak

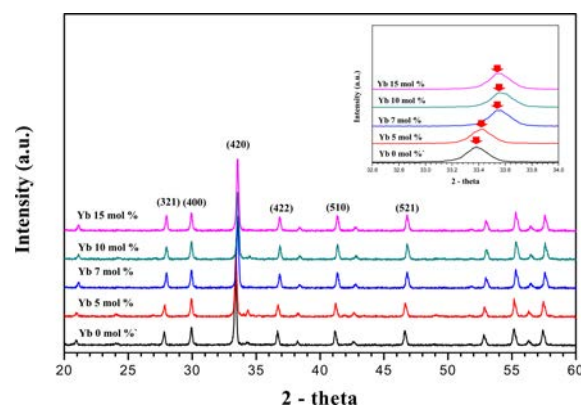


Fig. 2. XRD patterns of Yb³⁺/Er³⁺ co-doped YAG samples calcined at 1000 °C for 5 hrs as a function of Yb³⁺ concentration when BaF₂ flux is 7 wt%. The inset represents that main diffraction peaks of (4 2 0) plane near 2θ = 33.5° shift to high angle with Yb³⁺ concentration.

(4 2 0) and existence of secondary peaks were examined. When the pure YAG phase was synthesized from 700 up to 900 °C with 7.0 wt% BaF₂, secondary XRD peaks around 28.4° were detected as shown in inset of Fig. 1(b). Moreover, relative intensity of diffraction peaks was improved as the heat-treatment temperature increase. The YAG sample synthesized at 1000 °C with 7.0 wt% BaF₂ shows single crystalline XRD peaks without any secondary or unreacted phase. Fig. 1(a,b) indicate that the optimum synthesis condition using solid state reaction for pure YAG is 1000 °C with 7 wt% BaF₂ flux.

Fig. 2 shows the phase analysis of Yb³⁺/Er³⁺ co-doped YAG samples calcined at 1000 °C for 5 hrs as a function of Yb³⁺ concentration when BaF₂ flux is 7 wt%. Er³⁺-doped YAG crystals are very popular due to their abundant energy level for laser oscillation or upconversion luminescence [13]. However, because Er³⁺ ions have a very low absorption cross-section of the ⁴I_{11/2} level under 980 nm excitation, Er³⁺ single-doped luminescent materials have a relatively low emission intensity and pump efficiency. In order to overcome these drawbacks and enhance the emission efficiency, Yb³⁺ ions are generally used as co-dopant ions because they have a large absorption cross-section around 980 nm and a possible effective energy transfer from Yb³⁺ to the activator ions through the multi photon process [14]. In this study, effects of Yb³⁺ concentration on the optical property of the YAG:Yb³⁺,Er³⁺ was investigated when the concentration of Er³⁺ is fixed at 25.0 mol%.

In Fig. 2, it can be seen that XRD patterns are in good agreement with the standard diffraction pattern of pure YAG (JCPDS No: 33-0040). No impurities or secondary phases could be identified, which is evidence that single phase Yb³⁺/Er³⁺ co-doped YAG with Er³⁺/Yb³⁺ concentrations up to 25.0/15.0 mol% can be obtained. These powders fundamentally maintained characteristics of cubic structure, which are not affected by the doped Er³⁺ and Yb³⁺ ions [15].

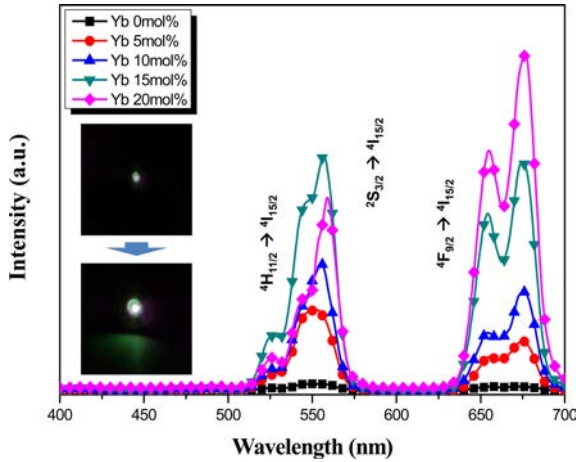


Fig. 3. Upconversion luminescent spectra of the Yb³⁺/Er³⁺ co-doped YAG samples as a function of Yb³⁺ concentrations from 0.0 to 20.0 mol% when concentration of Er³⁺ is fixed at 25.0 mol%. The photographs show Yb³⁺ undoped and 15.0 mol% doped YAG : Yb³⁺, Er³⁺ samples emit green light excited by a 980 IR laser (100 mW).

Based on the effective ionic radii of the cations, it can be expected that Er³⁺ and Yb³⁺ [$r(\text{Er}^{3+}) = 1.004 \text{ \AA}$, $r(\text{Yb}^{3+}) = 0.985 \text{ \AA}$, when CN = 8] are preferably substituted into the Y³⁺ sites [$r(\text{Y}^{3+}) = 1.019 \text{ \AA}$, when CN = 8] [16]. Note, that when the Y³⁺ ions are substituted by the Er³⁺ or Yb³⁺ ions, the corresponding lattice constant becomes smaller. Therefore, as shown in the inset in Fig. 2, with higher Yb³⁺ concentrations, the diffraction peaks are shifted to a high 2θ angle, which illustrates that Yb³⁺ ions were well substituted into Y³⁺ ion sites, resulting in reduction of lattice constants.

Fig. 3 shows room temperature upconversion luminescent spectra of the Yb³⁺/Er³⁺ co-doped YAG samples with Yb³⁺ concentrations ranging from without up to 20.0 mol% when the Er³⁺ concentration is fixed at 25.0 mol% under excitation at 980 nm. The upconversion luminescent spectra of the Yb³⁺/Er³⁺ co-doped YAG consisted of three regions [17]; (1) intense green emissions near 530 nm assigned to the ${}^2\text{H}_{11/2} \rightarrow {}^4\text{I}_{15/2}$ transition, (2) near 550 nm attributed to the ${}^4\text{S}_{3/2} \rightarrow {}^4\text{I}_{15/2}$ transition, and (3) relatively weak red emission around 660 and 670 nm attributed to the ${}^4\text{F}_{9/2} \rightarrow {}^4\text{I}_{15/2}$ transition, which contribute to the intra 4f-4f transitions of Er³⁺ ions.

The concentration dependence of upconversion emissions could be mainly attributed to the interactions between doping ions. As seen in Fig. 3, the upconversion emission intensity of green emissions near 530 and 550 nm and red emissions around 656 and 670 nm increased with increasing Yb³⁺ concentration up to 15.0 mol% and then decreased beyond the optimum doping concentration due to the concentration quenching effect [18]. The concentration quenching effect can be explained by the energy transfer between nearest Er³⁺ and Yb³⁺ ions. That is, with increasing Er³⁺ and Yb³⁺ ion

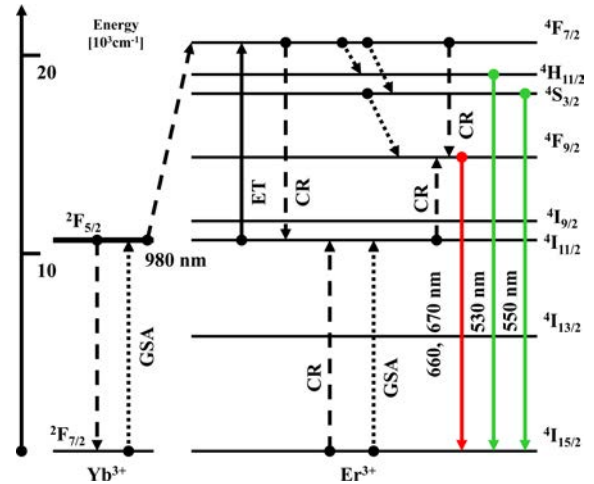


Fig. 4. Energy level diagram of Er³⁺ and Yb³⁺ in the YAG crystal and possible upconversion mechanism under excitation at 980 nm.

concentrations, the distance between Er³⁺ and Yb³⁺ ions will decrease, which can promote non-radiative energy transfer such as exchange interactions or multipole-multipole interactions [19]. Such a result is also observed from Er³⁺ doped or Yb³⁺/Er³⁺ co-doped in other host matrices [20]. Therefore, according to above mentioned results, it can be concluded that the optimum Yb³⁺ doping concentration is 15.0 mol% when concentration of Er³⁺ is 25.0 mol%. The Yb³⁺/Er³⁺ co-doped YAG specimen exhibited a stronger green emission shiny to the naked eye when excited by a 980 nm laser diode (100 mW) compared to the Yb³⁺ undoped YAG sample, as shown in inset of Fig. 3.

To comprehend the mechanism which populates the green (${}^2\text{H}_{11/2}$, ${}^4\text{S}_{3/2} \rightarrow {}^4\text{I}_{15/2}$) and red (${}^4\text{F}_{9/2} \rightarrow {}^4\text{I}_{15/2}$) luminescence, the upconversion mechanism and population processes for the Yb³⁺/Er³⁺ co-doped YAG system is schematically illustrated in Fig. 4. Under excitation at 980 nm, Er³⁺ and Yb³⁺ ions are initially excited from the ground state to the excited state through the ground state absorption (GSA) process ($\text{Er}^{3+} : {}^4\text{I}_{15/2} \rightarrow {}^4\text{I}_{11/2}$, $\text{Yb}^{3+} : {}^2\text{F}_{7/2} \rightarrow {}^2\text{F}_{5/2}$) or the energy transfer (ET) process of ${}^2\text{F}_{5/2}(\text{Yb}^{3+}) + {}^4\text{I}_{15/2}(\text{Er}^{3+}) \rightarrow {}^2\text{F}_{7/2}(\text{Yb}^{3+}) + {}^4\text{I}_{11/2}(\text{Er}^{3+})$ are responsible for the population at the ${}^4\text{I}_{11/2}$ level in Er³⁺. For the green emissions, there are three possible processes for the energy transition from the ${}^4\text{I}_{11/2}$ level to the ${}^4\text{F}_{7/2}$ level of Er³⁺, as follows [21].

$$\text{ESA: } {}^4\text{I}_{11/2} + \text{a photon (980 nm)} \rightarrow {}^4\text{F}_{7/2} \quad (1)$$

$$\text{ET: } {}^2\text{F}_{5/2}(\text{Yb}^{3+}) + {}^4\text{I}_{11/2}(\text{Er}^{3+}) \rightarrow {}^2\text{F}_{7/2}(\text{Yb}^{3+}) + {}^4\text{F}_{7/2}(\text{Er}^{3+}) \quad (2)$$

$$\text{ET: } {}^4\text{I}_{11/2}(\text{Er}^{3+}) + {}^4\text{I}_{11/2}(\text{Er}^{3+}) \rightarrow {}^4\text{F}_{7/2}(\text{Er}^{3+}) + {}^4\text{I}_{15/2}(\text{Er}^{3+}) \quad (3)$$

These three possible processes populate from the ${}^4\text{I}_{11/2}$

level to the ⁴F_{7/2} level in the Er³⁺ level, and then the ⁴F_{7/2} level relaxes rapidly and non-radiatively to the next lower levels at ²H_{11/2} and ⁴S_{3/2} in Er³⁺ because of short lifetime of the ⁴F_{7/2} level [22]. As a result, the above processes can produce green emissions in the spectral lines near 530 and 550 nm through the radiative transitions of ²H_{11/2}/⁴S_{3/2} → ⁴I_{15/2}. For the red emission, the ⁴F_{9/2} level is generated by non-radiative relaxation from the ⁴S_{3/2} to the ⁴F_{9/2} level and cross relaxation (CR) via the ⁴F_{7/2} + ⁴I_{11/2} → ⁴F_{9/2} + ⁴F_{9/2} transition in Er³⁺ [23]. Finally, the ⁴F_{9/2} level relaxes radiatively to the ground state at the ⁴I_{15/2} level and releases red emission at 660 and 670 nm, as shown in Fig. 3. The upconversion emission is dominated to strong green emission at 530 (²H_{11/2} → ⁴I_{15/2}) and 550 nm (⁴S_{3/2} → ⁴I_{15/2}) and the red emissions are very weak due to the weak absorption cross-section of the ⁴I_{13/2} level [24].

Summary

Effects of a flux (BaF₂) was investigated for the synthesis of Yb³⁺/Er³⁺ co-doped polycrystalline yttrium-aluminum garnet (YAG : Yb³⁺,Er³⁺) powder. It was found that the BaF₂ flux plays a key role in synthesizing the YAG : Yb³⁺,Er³⁺ powder in the solid state reaction process. The optimum synthesis temperature was 1000 °C when 7 wt% BaF₂ was used, which was lower than the reported synthesis temperature about 600 °C. Single phased YAG : Yb³⁺,Er³⁺ with Yb³⁺/Er³⁺ concentrations up to 20.0/25.0 mol% could be obtained without any impurities nor secondary phases. Under NIR excitation (980 nm), Yb³⁺/Er³⁺ co-doped YAG powder exhibited obviously bright green upconversion luminescence at 530 and 550 nm with weak red emission at 660 and 670 nm. It was found that the upconversion emission intensity depends on Yb³⁺ acting as a sensitizer ion to improve the absorption cross-section around 980 nm, while Er³⁺ acts as an activator ion for upconversion luminescent centers in the YAG matrix. The optimum doping concentrations of Yb³⁺ for highest green upconversion luminescence were 15.0 mol% when concentration of Er³⁺ was fixed at 25.0 mol%.

References

1. Y.X. Pan, M.M. Wu, and Q. Su, J Phys. Chem. Sol. 65 (2004) 845-850.
2. E. F. Schubert and J. K. Kim, Science 308 (2005) 1274-1278.
3. I. Warshaw, R. Roy, J. Am. Ceram. Soc. 42 (1959) 434-439.
4. J.S. Abell, I.R. Harris, B. Cocakayne, B. Lent. J. Mater. Sci. 9 (1974) 527-540.
5. N. Daikuzono, Review of Laser Eng. 21 (1993) 173-203.
6. N. Daikuzono, S.N. Joffe, Medical Int. 19 (1985) 173-178.
7. H. Yagi, T. Yanagitani, T. Numazawa, K. Ueda, Ceram. Int. 33 (2007) 711-715.
8. J.S. Kim, P. E. Jeon, J.C. Choi, H.L. Park, S.I. Mho, and G.C. Kim, Appl. Phys. Let. 84 (2004) 2931-2933.
9. Q. Zhang, F. Saito, Powder Technol. 129 (2003) 86-91.
10. Y.X. Pan, M.M. Wu, Q. Su, Master. Sci. Eng. B. 106 (2004) 251-255.
11. S.H. Lee, H.Y. Koo, D.S. Jung, J.M. Han, Y.C. Kang, Opt. Mater. 31 (2009) 870-876
12. S. Xu, L. Sun, Y. Zhang, H. Ju, S. Zhao, D. Deng, H. Wang, B. Wang, J. Rare Ear. 27 (2009) 327-333.
13. Y.C. Kang, H.S. Roh, S.B. Park, Adv. Mater. 12 (2000) 451-456.
14. H.X. Yang, H. Lin, Y.Y. Zhang, B. Zhai and E.Y.B. Pun, J. Alloy. Compd. 453 (2008) 493-497.
15. J. Liu, H. Lian and C. Shi, Opt. Mater. 29 (2007) 1591-1595.
16. R. D. Shannon, Acta Cryst. A. 32 (1976) 751-760.
17. X.X. Luo and W.H. Cao, J. Mater. Res. 23 (2008) 2078-2081.
18. D. Yang, C. Li, G. Li, M. Shang, X. Kang and J. Lin, J. Mater. Chem. 21 (2011) 5923-5928.
19. H. Guo, N. Dong, M. Yin, W. Zhang, L. Lou and S. Xia, J. Phys. Chem. B 108 (2004) 19205-19209.
20. Y. Bai, K. Yang, Y. Wang, X. Zhang and Y. Song, Opt. Comm. 281 (2008) 2930-2940.
21. N.M. Sangeetha and F.C.J.M. van Veggel, J. Phys. Chem. C 33 (2009) 14702-14707.
22. F. Auzel, Chem. Rev. 104 (2004) 139-149.
23. F. Wang and X. Liu, Chem. Soc. Rev. 38 (2009) 976-980.
24. G.Y.Chen, H.C. Liu, H.J. Liang, G. Somesfalean and Z.G. Zhang, Solid State Commun. 196 (2008) 148-155.
25. H.J. Kim, D.J. Kim, J.T. Hong, G.C. Xu, D.G. Lee, J. Elect. Eng. Tech. 4 (2011) 275-279.
26. S.J. Park, S.J. Park, H.Y. Park, J.W. Park, J.Y. Sim, J.Y. Choi, H.J. Kim, J. Elect. Eng. Tech. 2 (2007) 112-117.
27. J. Raja, C. Christiber, J. Elect. Eng. Tech. 2 (2010) 552-560.
28. M.Y. Kim, D.S. Bae, kor. J. Mat. Res. 23 (2013) 31-34.